GPS Solutions (2021) 25:51
https://doi.org/10.1007/s10291-020-01081-z

ORIGINAL ARTICLE

Endpoint-based optimal fractal interpolation for predicting BDS-3 system time offsets

Tao Han[1] · **Decai Zou**[2]

Received: 24 March 2020 / Accepted: 27 December 2020 / Published online: 9 February 2021

Abstract

In order to improve the interoperability within the Global Navigation Satellite System (GNSS), the International Committee on Global Navigation Satellite Systems published a joint statement in December 2019 that stated that all GNSS providers agree to monitor and broadcast the time offsets between each system timescale and the Universal Time Coordinated (UTC) or the rapid realization of UTC (UTCr). This commitment requires the study of precise prediction models for system time offsets. The prediction model of system time offsets is different from that of the atomic clock because of the control of the system timescale. The offsets between the system time of the Beidou Satellite Navigation System-3 (BDS-3) and the National Time Service Center (NTSC), called [UTC(NTSC)-BDT], have two main periods of 12 h and 24 h, according to the Fast Fourier Transform analysis. The rescaled range (R/S) analysis demonstrates that it has long memory, making it a fractal time series with a memory period of about 10.4 h. While using the fractal interpolation method to predict the [UTC(NTSC)-BDT] series, we found that the prediction error reaches its minimum value if adding disturbance on the estimated endpoint of the forecasted interval. After verifying the correlation between the estimated endpoints with the minimal interpolation error and minimal prediction error and proving the existence and uniqueness of the estimated endpoint with the minimal interpolation error, we established the endpoint-based optimal fractal interpolation prediction method. The experimental results indicate that the average prediction accuracy of the proposed prediction model is improved by 57.90% and 39.26% compared to that of a quadratic model and standard fractal prediction model, respectively. The accuracy analysis results of numerical tests indicate that the proposed prediction model can restrain the divergence of prediction error. Finally, we transform the [UTC(NTSC)-BDT] into [UTCr-BDT] using the [UTCr-UTC(NTSC)] published by the Bureau International des Poids et Mesures (BIPM) to meet the requirement of GNSS interoperability. The prediction accuracies of daily [UTCr-BDT] using the proposed prediction model are no more than 1.5 ns with uncertainty about 6 ns.

Keywords BDS-3 · System time offsets · Long-memory · Fractal prediction · Optimal

Introduction

Compatibility and interoperability are main principles in the BeiDou Navigation Satellite System (BDS) construction and development. The BDS will enhance the compatibility and interoperability with other navigation satellite systems to provide global positioning, navigation and timing services (Yang et al. 2011). The time offsets among multi-systems is a key component of the Global Navigation Satellite System (GNSS) compatibility and interoperability (Yang et al. 2016). It is also the most important content of GNSS interoperability parameters (Han et al. 2013). Monitoring and forecasting the system time offsets will be important for realizing the GNSS interoperability. For this reason, the Bureau International des Poids et Mesures (BIPM), i.e., the International Bureau of Weights and Measures, is broadcasting monitored results of daily time offsets for GPS and GLONASS every month; and it will broadcast the time offsets of Galileo positioning system and BDS in the near future (ICG Secretariat 2019).

Monitoring the system time offsets alone does not meet the user requirement; prediction of time offsets is

✉ Tao Han
hantao@xaut.edu.cn

[1] Department of Applied Mathematics, School of Sciences, Xi'an University of Technology, Xi'an 710048, Shaanxi, China

[2] National Time Service Center, Chinese Academy of Sciences, Xi'an 710600, Shaanxi, China

necessary for multi-system user applications (Han et al. 2017). Research on the prediction model of system time offsets is a prerequisite for realizing GNSS interoperability. Presently, the common time offsets prediction methods are mainly based on a polynomial model, and the prediction accuracy is improved through various modification models. Examples include the Grey Model (GM) combined polynomial model (Zhang et al. 2014a), autoregressive combined polynomial model with periodic terms (Fu et al. 2015), and Kalman filter to estimate the polynomial coefficients (Zhu et al. 2016). Recently, fractal theory was applied to GNSS time offsets prediction. After the fractal behavior of GNSS time offsets was proven, Han et al. (2018) used the fractal interpolation model to predict GNSS time offsets. A fractal series is defined as having self-similarity on different scales; this long-term memory is the basis of our mathematical approach. This is the first time the fractal theory was used to discuss the prediction method of GNSS time offsets. However, further ways to improve prediction accuracy using this method are yet to be discovered.

The main purpose of this research is to discuss the principles and methods to improve the forecast precision of GNSS time offsets using a fractal prediction model. The study object of this study is the time offsets between the BDS time (BDT) and the Universal Time Coordinated (UTC), which is provided by the National Time Service Center (NTSC) of China. A spectral analysis was conducted that showed the [UTC(NTSC)-BDT] time series has two significant cycle terms. The main period is 12 h, and the second period is 24 h. The rescaled range (R/S) analysis result showed that the [UTC(NTSC)-BDT] time series has obvious fractal characteristics and long-term memory, with a memory span of about 10.4 h. When repeating the prediction algorithm proposed in Han et al. (2018), we found the endpoint estimation effects on the prediction accuracy. The prediction error met its minimum value when a small disturbance was added to the estimated endpoint. This phenomenon sparked our interest. In order to find the estimated endpoint for this minimal prediction error, the following two steps were considered in this work. The first step was to verify the correlation between the estimated endpoint corresponding to the minimum interpolation error and that corresponding to the minimum prediction error. The second step was to prove the existence and uniqueness of the estimated endpoint corresponding to the minimum interpolation error. Based on these two steps, we first calculated the endpoint corresponding to the minimum interpolation error, and then estimated the endpoint corresponding to the minimum prediction error according to the correlation between the two estimated endpoints. Then, the endpoint based optimal fractal interpolation model for BDS system time offsets prediction can be found.

BDS time offsets analysis

BDT is not directly aligned with UTC. It aligns with UTC(NTSC), which aligns with UTC (Yang et al. 2019). The NTSC monitors the time offsets between BDT and UTC(NTSC) (denote as [UTC(NTSC)-BDT]) (Zhang et al. 2014b; Guang et al. 2018). The [UTC(NTSC)-BDT] time series observed at the NTSC is shown in Fig. 1.

The blue curve shown in Fig. 1 is the [UTC(NTSC)-BDT] time series. The data sampling period is 16 min, and there are 90 observations per day. The uncertainties of the BDT offsets range from 0.075 to 0.48 ns, calculated by day; and the uncertainty of this series is about 4.59 ns.

Periodic term detection

The relationship between the reference timescale and GNSS tine (GNSST) can always be described as a quadratic polynomial (Wu 2011). The BDS time offsets monitored by the NTSC are calculated by day. Thus, the [UTC(NTSC)-BDT] within each day is described as the quadratic polynomial (Gao et al. 2011):

$$x(t) = a_0 + a_1(t_i - t_0) + a_2(t_i - t_0)^2 + \Delta_i \quad (1)$$

The parameters ($a_i, \quad i = 0, 1, 2$) are the time offset, frequency offset, and frequency. t_0 is the reference epoch of the time offsets model, t_i is the observation epoch, and $x(t)$ is the time offsets observation. Δ_i denotes the model residual. The quadratic residual of [UTC(NTSC)-BDT] is shown as Fig. 2 (top), which is calculated by day. The main purpose in this section is to detect the periodic term rather than quadratic coefficient estimation; therefore the post-processed method is employed. The quadratic parameters of future data should be estimated via the known data in real-time applications.

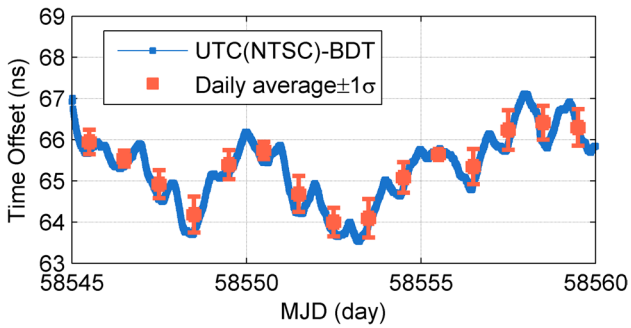

Fig. 1 BDS system time offsets data from MJD 58,545 to 58,559 (half month). The error bar reflect the daily average of [UTC(NTSC)-BDT] 1-sigma bars. The [UTC(NTSC)-BDT] comes from NTSC monitoring results

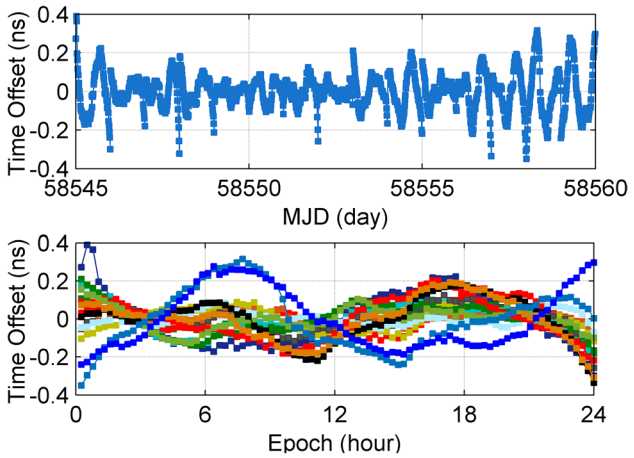

Fig. 2 Fitting [UTC(NTSC)-BDT] using quadratic model. Top: residual series of half month. Bottom: sum of each day's fitted 12 and 24-h curves to the residuals of fit

In Fig. 2 (bottom), the periodic phenomena of the fitting residual are obvious. In order to detect the periodic terms of [UTC(NTSC)-BDT] based on the given data, the Fast Fourier Transform algorithm was used, and the analysis result is shown in Fig. 3. Meanwhile, it is noticeable that two of the days in the analysis have different phases and amplitudes compared to all of the others. They are the last two days. After review, the main reason for the two days of different phases and amplitudes is that one satellite for the time comparing was lost lock from March 16, 2019, i.e., MJD 58,558. Thus, there is more noise in the last two days of data since lack of data from one satellite, but the periodic term did not change in frequency.

From the top panel of Fig. 3, it can be seen that there are two significant and special periodic terms in [UTC(NTSC)-BDT], the main period is about 12 h and the second period is around 24 h. In the lower panel of Fig. 3, it can be seen that the periodic terms in the first 13 days are the same to what in the last two days. Furthermore, the increased amplitude in the last two days indicates that the lack of observations makes the observation noise increased. Since these periodic terms are similar to not only the orbital period of BDS satellites, but also the period of multipath effects of signals from the BDS GEO/IGSO satellites. This indicates that the [UTC(NTSC)-BDT] time series discussed here contains periodic noise caused by BDS satellites orbit and the multipath effects. The purpose of this paper is to discuss the possibility of using fractal method to predict GNSS time offsets and the mathematical techniques to improve the prediction accuracy, we are concerned only with the mathematical aspects of the analysis, and the physical significances of the results are outside of the scope of the discussion. In order to obtain the pure time offsets, the [UTC(NTSC)-BDT] time offsets model can be presented as (Huang et al. 2014):

$$x(t) = a_0 + a_1(t_i - t_0) + a_2(t_i - t_0)^2 + \sum_{j=1}^{n} A_j \sin[2\pi f_j(t_i - t_0) + \varphi_j] + \Delta_i \quad (2)$$

where A_j, f_j and φ_j are the amplitude, frequency, and phase of the time offsets period in the j th of n periods, respectively. The fitting residual of [UTC(NTSC)-BDT] with two significant periodic terms is shown in Fig. 4; and the values of the fitted parameters with their uncertainties and the residuals are shown in Table 1 and Fig. 5.

Comparing Figs. 2 and 4, it can be seen that the fitting residual after adding two periodic terms is more stable than using the quadratic model alone. The accuracy of the fit is significantly improved as evidenced from a reduced RMS of 0.1509 ns to 0.0633 ns. This improvement also verifies the existence of the periodic term in the [UTC(NTSC)-BDT] time series.

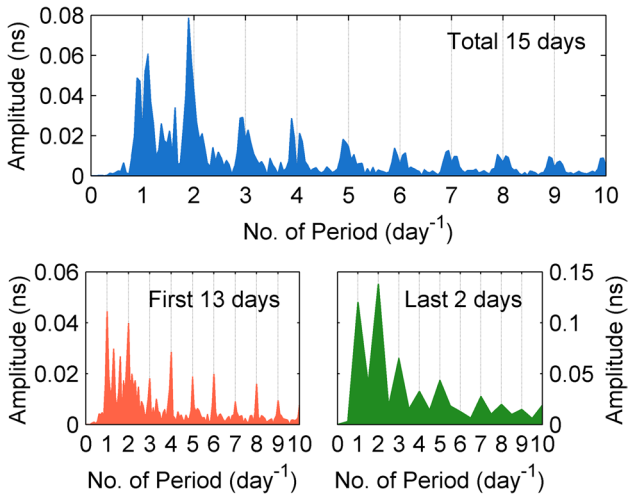

Fig. 3 Frequency analysis of the [UTC(NTSC)-BDT]. The main period is about 12 h, and the second period is about 24 h

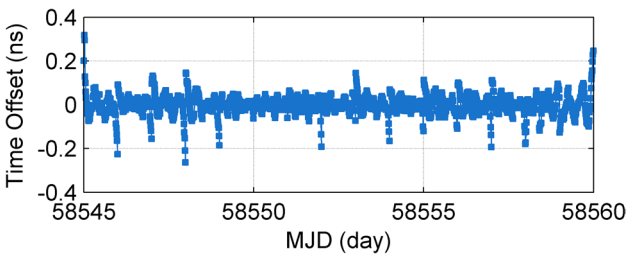

Fig. 4 Fitting residual of the [UTC(NTSC)-BDT] quadratic model with two periodic terms

Table 1 Values of the fitted parameters with their uncertainties and the residuals of [UTC(NTSC)-BDT] using Eqs. (1) and (2)

MJD	Quadratic model				Quadratic model + periodic terms			
	Value ± uncertainty			Residual	Value ± uncertainty			Residual
	a_0	a_1	a_2 (10^{-3})	rms (ns)	A_1	A_2		rms (ns)
58,545	66.69 ± 0.09	−0.134 ± 0.018	4.492 ± 0.712	0.143	0.086 ± 0.033	0.128 ± 0.033		0.073
58,546	65.66 ± 0.03	−0.063 ± 0.007	3.308 ± 0.260	0.052	0.017 ± 0.017	0.044 ± 0.017		0.037
58,547	65.86 ± 0.05	−0.170 ± 0.011	5.728 ± 0.442	0.089	0.083 ± 0.028	0.037 ± 0.0282		0.063
58,548	64.59 ± 0.05	−0.167 ± 0.010	8.295 ± 0.399	0.080	0.027 ± 0.025	0.070 ± 0.025		0.056
58,549	65.22 ± 0.02	−0.045 ± 0.004	3.689 ± 0.160	0.032	0.029 ± 0.010	0.005 ± 0.011		0.024
58,550	66.32 ± 0.04	−0.114 ± 0.007	4.093 ± 0.292	0.059	0.076 ± 0.010	0.010 ± 0.010		0.022
58,551	65.91 ± 0.04	−0.243 ± 0.008	8.800 ± 0.329	0.066	0.060 ± 0.018	0.034 ± 0.018		0.040
58,552	64.97 ± 0.02	−0.161 ± 0.004	5.067 ± 0.170	0.034	0.021 ± 0.012	0.017 ± 0.012		0.027
58,553	63.73 ± 0.05	−0.033 ± 0.010	3.923 ± 0.384	0.077	0.049 ± 0.020	0.067 ± 0.020		0.045
58,554	64.92 ± 0.07	−0.050 ± 0.013	3.917 ± 0.527	0.106	0.099 ± 0.014	0.078 ± 0.014		0.031
58,555	65.58 ± 0.04	0.020 ± 0.007	−0.954 ± 0.295	0.060	0.031 ± 0.020	0.045 ± 0.020		0.044
58,556	65.42 ± 0.07	−0.106 ± 0.014	6.231 ± 0.564	0.115	0.130 ± 0.021	0.052 ± 0.021		0.047
58,557	66.03 ± 0.07	−0.067 ± 0.014	5.174 ± 0.545	0.110	0.110 ± 0.019	0.071 ± 0.019		0.042
58,558	67.51 ± 0.10	−0.206 ± 0.019	7.191 ± 0.768	0.420	0.315 ± 0.067	0.368 ± 0.067		0.151
58,559	66.97 ± 0.10	−0.048 ± 0.020	−0.485 ± 0.779	0.311	0.245 ± 0.048	0.260 ± 0.048		0.108

Long memory of BDS time offsets

While analyzing the fractal behavior of [UTC-GPST] and [UTC-GLOT], Han et al. (2018) supposed that the fractal behavior may be universal in GNSS time offsets. A long memory of time series means that there is a type of persistence or long-term range dependence in the fluctuation of time series; that is, there is a significant autocorrelation between the former data and the current data in a fractal time series. The former data will have a continuous impact on the fluctuation of the current data, which gives the time series certain predictability. The R/S analysis was first proposed by Hurst (1951). The Hurst exponent H is a criterion to identify this systematic nonrandom feature. The calculation process is as follows:

(1) Separate a time offsets time series $\{x_i\}$ with length N into M continuous subsequences of length n. Denote each subsequence as I_m, $m = 1, 2, \cdots, M$. Then, each element in I_m is denoted as $x_{k,m}$, $k = 1, 2, \cdots, n$ and $m = 1, 2, \cdots, M$.

(2) Compute the mean value e_m and the cumulative mean deviation $x_{k,m}$ of every subsequence I_m:

$$e_m = \frac{1}{n}\sum_{k=1}^{n} x_{k,m} \tag{3}$$

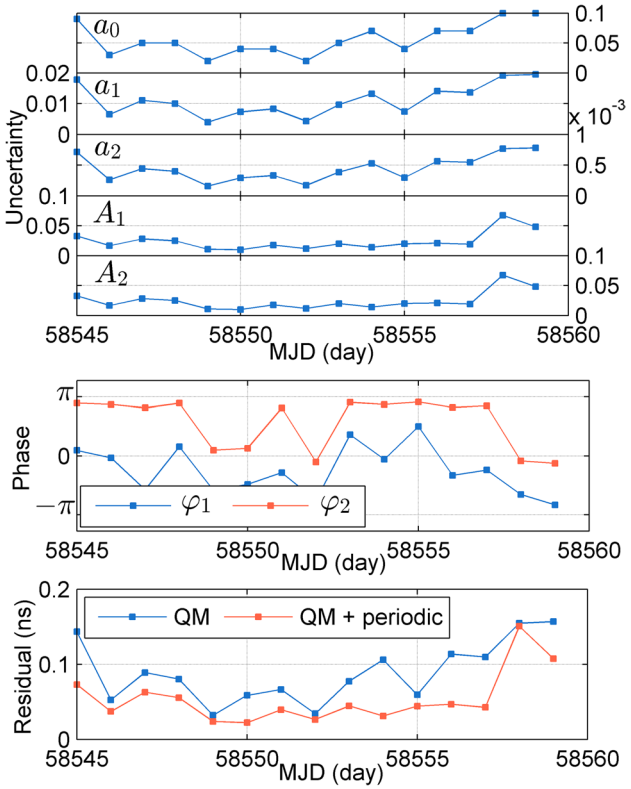

Fig. 5 Uncertainties fitted parameters and the fitting residual. Top: the uncertainties of five fitted parameters of equation (2) in each day. Middle: the phases of the first two main periodic terms. Bottom: the fitting residual of [UTC(NTSC)-BDT] using quadratic model and quadratic model with two periodic terms respectively

$$X_{k,m} = \sum_{i=1}^{k} (x_{i,m} - e_m), \quad k = 1, 2, \cdots, n \tag{4}$$

(3) According to (4), the mean value of a cumulative mean deviation series $\{X_{1,m}, X_{2,m}, \cdots, X_{n,m}\}$ is zero. Define the range of subsequences I_m as:

$$R_{I_m} = \max(X_{k,m}) - \min(X_{k,m}), \quad k = 1, 2, \cdots, n \tag{5}$$

(4) Compute the standard deviation S_{I_m} and rescale/standardize it as R_{I_m}/S_{I_m}:

$$S_{I_m} = \sqrt{\frac{1}{n}\sum_{k=1}^{n} (x_{k,m} - e_m)^2} \tag{6}$$

(5) The mean rescaled range of the M subsequence I_m with length n is:

$$(R/S)_n = \frac{1}{M}\sum_{m=1}^{M} \left(R_{I_m}/S_{I_m}\right) \tag{7}$$

(6) Repeat the above steps with a different divided length (i.e. the different time scale) n; more mean rescaled range values can be obtained. There is a power-law relationship between n and $(R/S)_n$:

$$(R/S)_n = c \cdot n^H \tag{8}$$

Alternatively, we can say there is linear relationship between $\log(R/S)_n$ and $\log n$:

$$\log(R/S)_n = c + H \log n \tag{9}$$

(7) Use the double logarithm regression for n and $(R/S)_n$. The slope is the long-range correlation parameter, the so-called Hurst exponent H. Furthermore, the long-range correlation parameter H of the time offsets can be estimated using the least square method.

The Hurst exponent can not only distinguish fractal time series from random time series, but also determine the persistence or anti-persistence of a fractal time series. A time series with $H = 0.5$ is a random sequence. A time series with a Hurst exponent in the range (0.5, 1) is a long-memory time series. It means that if an element is bigger (smaller) than the previous one, the next element will probably be bigger (smaller) than this element. The closer the Hurst exponent is to 1, the more likely this is. Otherwise, a time series is an anti-persistence sequence when $0 < H < 0.5$. It means that if an element is bigger (smaller) than the previous one, the next element will probably be smaller (bigger) than this element. The closer the Hurst exponent is to 0, the more likely this is.

However, for any long-memory time series, its long-term correlation is not endless, but has an average length called the memory span. The correlation between two elements in a long-memory time series will be significantly weakened when the time interval between them exceeds this memory span. That is to say, for a long-memory time series, when the length of the subsequence is sufficiently long, H will be less than 0.5. In this case, the subsequence length n_0, which makes $H = 0.5$, is known as the memory span. The memory span n_0 is estimated by constructing the V statistic as follows:

$$V = \frac{(R/S)_n}{\sqrt{n}} \tag{10}$$

Substitute equation (8) into (10) and take a derivative with respect to n:

$$\frac{dV}{dn} = \frac{d\left(c \cdot n^{H-0.5}\right)}{dn} = c(H - 0.5)n^{H-1.5} \tag{11}$$

Then, $dV/dn = 0$ if $H = 0.5$, i.e. the V statistic curve meets the extreme point at n_0. The R/S analysis result and V statistic curve of the [UTC(NTSC)-BDT] are shown in Fig. 6.

As shown in Fig. 6 (right), the V statistic curve of [UTC(NTSC)-BDT] meets its extreme point at $\ln n_0 = 2.3418$, and the corresponding memory span is:

$$n_0 = \exp\left(\ln n_0\right) = 10.4 \text{ h} \tag{12}$$

The curve of $\log(R/S)_n$ versus $\log n$ and the fitted lines of the $\log(R/S)_n - \log n$ curve before and after the memory-span are shown in Fig. 6 (left). The two fitted lines are:

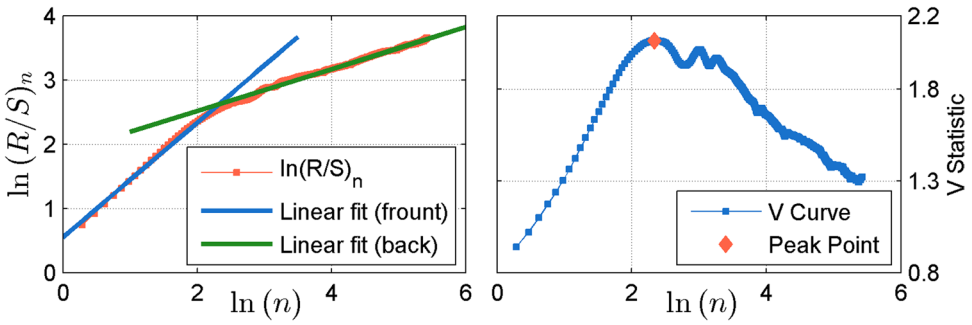

Fig. 6 Rescaled range analysis result (left) and V statistic curve (right) of [UTC(NTSC)-BDT]

$$\ln(R/S)_n = \begin{cases} 0.89\ln n - 0.63, & n \le 10.4\text{ h} \\ 0.33\ln n + 1.43, & n > 10.4\text{ h} \end{cases} \tag{13}$$

When $n \le 10.4$ h, the Hurst exponent of [UTC(NTSC)-BDT] is $0.89 > 0.5$, and the BDS time offsets series shows strong long memory. When $n > 10.4$ h, the Hurst exponent is $0.33 < 0.5$, thereby indicating that the [UTC(NTSC)-BDT] series shows anti-persistence. The R/S analysis results above show that the [UTC(NTSC)-BDT] series is a fractal time series with long memory, and it is feasible to use fractal theory to study the prediction method.

Fractal prediction of BDS time offsets

The basic principle of fractal interpolation prediction is to construct an iterative function system by the given fractal set, then extend its domain in time, so that the extended iterative function system can inherit the fractal characteristics of the original fractal set. In a given fractal interpolation set $\{(t_i, x_i) \in \boldsymbol{R}^2 | i = 0, 1, 2, \cdots, N\}$ ($t_i < t_j$ when $i < j$), the curve of the fractal interpolation function $\Gamma : [t_0, t_N] \to \boldsymbol{R}$ passes through all the points of this fractal set. This curve is the attractor of an iterative function system generated by affine transformations.

The model

The following affine transformation $\omega_i : [t_0, t_N] \times \boldsymbol{R} \to \boldsymbol{R}$ is frequently applied to generate the affine iterative function system $\{\boldsymbol{R}^2; \omega_i, i = 1, 2, \cdots, N\}$:

$$\omega_i(t, x) = \big(L_i(t), F_i(t, x)\big) \tag{14}$$

It satisfies $\omega_i(t_0, x_0) = (t_{i-1}, x_{i-1})$ and $\omega_i(t_N, x_N) = (t_i, x_i)$, when

$$\begin{cases} L_i(t) = a_i t + e_i \\ F_i(t, x) = c_i t + \mu_i x + f_i = \phi_i(t) + \mu_i x \end{cases} \tag{15}$$

The parameters are calculated as follows:

$$\begin{cases} a_i = \dfrac{t_i - t_{i-1}}{t_N - t_0} \\ e_i = \dfrac{t_N t_{i-1} - t_0 t_i}{t_N - t_0} \\ c_i = \dfrac{x_i - x_{i-1} - \mu_i(x_N - x_0)}{t_N - t_0} \\ f_i = \dfrac{t_N x_{i-1} - t_0 x_i - \mu_i(t_N x_0 - t_0 x_N)}{t_N - t_0} \end{cases} \tag{16}$$

The free parameters $\mu_i \in (-1, 1)$ are called the vertical scaling factors, which can be obtained using an analytic method (Mazel and Hayes (1992) or a geometric method (Han et al. 2018). To extend the iterative function system, we define ω_{N+1} as:

$$\begin{aligned} \omega_{N+1}(t, x) &= \begin{pmatrix} L_{N+1}(t) \\ F_{N+1}(t, x) \end{pmatrix}^T \\ &= \begin{pmatrix} a_{N+1} t + e_{N+1} \\ c_{N+1} t + \mu_{N+1} x + f_{N+1} \end{pmatrix}^T \\ &= \begin{pmatrix} a_{N+1} t + e_{N+1} \\ \phi_{N+1}(t) + \mu_{N+1} x \end{pmatrix}^T \end{aligned} \tag{17}$$

and the parameters are:

$$\begin{cases} a_{N+1} = \dfrac{t_{N+1} - t_N}{t_{N+1} - t_0} \\ e_{N+1} = \dfrac{t_{N+1} t_N - t_0 t_{N+1}}{t_{N+1} - t_0} \\ c_{N+1} = \dfrac{\hat{x}_{N+1} - x_N - \mu_{N+1}(\hat{x}_{N+1} - x_0)}{t_{N+1} - t_0} \\ f_{N+1} = \dfrac{t_{N+1} x_N - t_0 \hat{x}_{N+1} - \mu_{N+1}(t_{N+1} x_0 - t_0 \hat{x}_{N+1})}{t_{N+1} - t_0} \end{cases} \tag{18}$$

After extending the fractal interpolation function Γ to the interval $[t_0, t_{N+1}]$ using $\omega_{N+1} : [t_N, t_{N+1}] \times \boldsymbol{R} \to \boldsymbol{R}$, the forecasted time offsets in $[t_N, t_{N+1}]$ can be obtained. The vertical scaling factors μ_{N+1} in $[t_N, t_{N+1}]$ and the estimated $\hat{X}_{N+1}$ at t_{N+1} can be calculated according to Han et al. (2018).

Numerical example and discussion

Using the previous [UTC(NTSC)-BDT] time series as the observation, the prediction lengths are 1 h, 3 h, 6 h, and 12 h. The prediction results of [UTC(NTSC)-BDT] using the fractal prediction method in Han et al. (2018) are shown in Fig. 7, and the prediction accuracies can be found in Table 2.

In the prediction process, we found that the prediction accuracy changes when adding a small disturbance Δx on $\hat{x}_{N+1}$; and there is a minimal prediction residual during this change, as shown in Fig. 8.

The phenomenon shown in Fig. 8 is of great importance to us. It shows that it is possible to improve the prediction accuracy by changing the value of $\hat{x}_{N+1}$. Although we can get the prediction error in the numerical experiment, we cannot obtain the prediction error in the actual applications. Thus, our discussion will focus on how to use known conditions to estimate the disturbance of the endpoint, which corresponds to the optimal (suboptimal) prediction accuracy. In order to solve this problem, two questions are posed here: first, whether there is a correlation between Δx for the optimal prediction error and $\Delta x'$ for the optimal interpolation

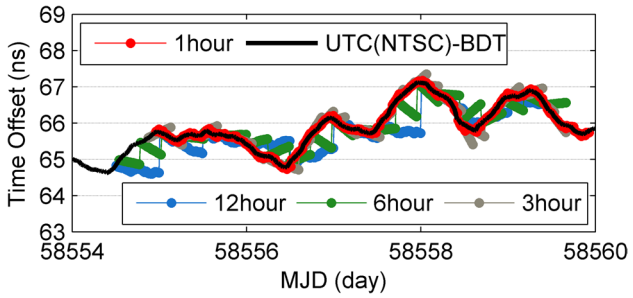

Fig. 7 Prediction results of [UTC(NTSC)-BDT] shown as Fig. 1 using the standard fractal interpolation prediction method. The fitting lengths are more than 104 h, which is 10 times the memory span obtained by (12)

Table 2 Prediction accuracies of [UTC(NTSC)-BDT] using the standard fractal interpolation prediction method in different prediction lengths

1 h	3 h	6 h	12 h
rms(ns)			
0.036	0.124	0.312	0.473

error; second, whether there is a unique optimal solution for the interpolation error when the endpoint disturbance $\Delta x'$ changes.

Endpoint-based optimal fractal interpolation prediction method

The two questions proposed in the previous section are the key to improve the fractal prediction accuracy. The answer to question one is helpful for us to estimate the optimal prediction error by interpolating points defined by the given time offsets series. The answer to question two will help us to calculate the endpoint disturbance $\Delta x'$ of the optimal interpolation error. There is a close relationship between these two questions. If their answers are both positive, then the prediction accuracy can be further improved.

A correlation between endpoint disturbances for the minimal error of prediction and interpolation indicates that when the interpolation error in interval $[t_0, t_N]$ is at a minimum value, the endpoint disturbance at $\hat{x}_{N+1}$ is $\Delta x'$. Consider Δx as the endpoint disturbance at $\hat{x}_{N+1}$ of the minimum prediction error in interval $[t_N, t_{N+1}]$. First, we will calculate Δx and $\Delta x'$ when the prediction length is 1 h, 3 h, 6 h, and 12 h. Then, correlation analysis and linear regression will be performed.

Figure 9 shows that the four Pearson correlation coefficients are greater than 0.6; this indicates a strong connection between disturbances $\Delta x'$ and Δx. Notably, for the 12 h prediction, a 0.85 correlation coefficient shows a strong uphill (positive) linear relationship between the two disturbances.

Figure 10 shows scatter plots of $\Delta x'$ verse Δx. The fitted line of the two endpoint disturbances shows that there is a linear relationship between them, and the regression equations are:

$$\Delta x' = \begin{cases} 1.08\Delta x + 0.01, & 1\text{ h}; \\ 0.99\Delta x + 0.02, & 3\text{ h}; \\ 0.80\Delta x + 0.08, & 6\text{ h}; \\ 0.53\Delta x + 0.16, & 12\text{ h}. \end{cases} \tag{19}$$

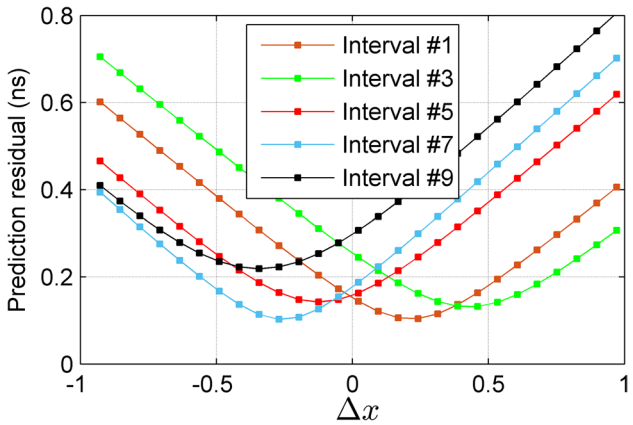

Fig. 8 Prediction residual curves of [UTC(NTSC)-BDT] when adding disturbance Δx on the estimated endpoint. Using the 1st, 3rd, 5th, 7th and 9th prediction intervals as examples, the prediction length is 12 h

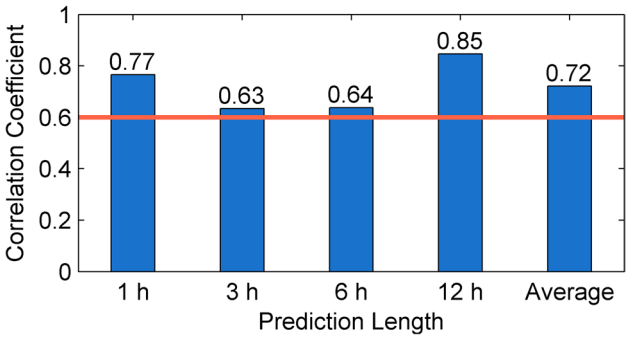

Fig. 9 Pearson correlation coefficients between Δx and Δx' in different prediction lengths

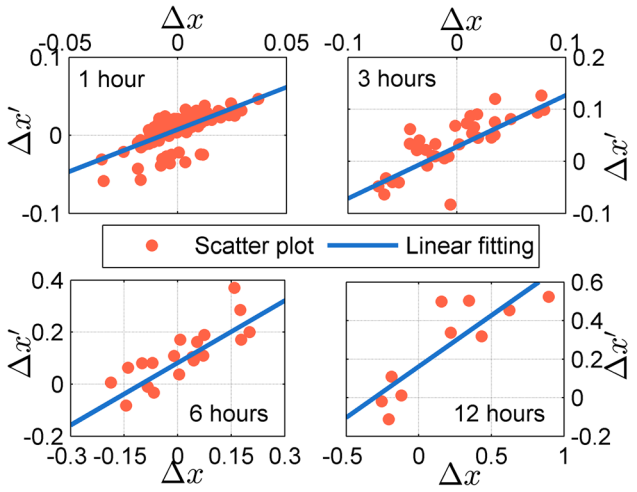

Fig. 10 Linear fit of endpoint disturbances for optimal prediction and interpolation error in different prediction lengths

Thus, it is possible to estimate Δx with the value of the minimal interpolation endpoint disturbance $\Delta x'$. Moreover, the estimated endpoint $\hat{X}_{N+1}$ will be corrected.

Existence and uniqueness of estimated endpoint for minimal interpolation error

The next question is whether the minimum interpolation error exists and is solvable and whether the corresponding endpoint disturbance $\Delta x'$ is unique. Discussing the endpoint disturbance $\Delta x'$ and discussing the estimated endpoint $\tilde{x}_{N+1} = \hat{x}_{N+1} + \Delta x'$ are equivalent.

According to the definition of the fractal interpolation function, the $\Gamma(t)$ curve passes through all the interpolation points. So $\Gamma(t)$ is formed by all the interpolation points in $[t_0, t_N]$. Consider the fractal interpolation function in $[t_0, t_{N+1}]$ with the estimated endpoint $\tilde{x}_{N+1}$ as $\Gamma(t, \tilde{x}_{N+1})$. In order to minimize the interpolation error caused by $\tilde{x}_{N+1}$, it is required that $\Gamma(t, \tilde{x}_{N+1}) - \Gamma(t)$ with $(t \in [t_0, t_N])$ be the minimum. We will take two iterations as an example. More detailed computing can be found in the appendix.

Fractal interpolation value

The initial point $P_0(t^*, x^*)$ of the iterative function system is mapped into $\omega_i(P_0)$ by mapping ω_i of $[t_{i-1}, t_i]$. Then, it is mapped into $\omega_j(\omega_i(P_0))$ by mapping ω_j of $[t_{j-1}, t_j]$ as shown in equations

$$\begin{aligned}\omega_j\big(\omega_i(t^*, x^*)\big) &= \omega_j\big(L_i(t^*), F_i(t^*, x^*)\big) \\ &= \big(L_j\big(L_i(t^*)\big), F_j\big(L_i(t^*), F_i(t^*, x^*)\big)\big)\end{aligned} \tag{20}$$

and

$$\begin{cases} L_j\big(L_i(t^*)\big) = a_j(a_i t^* + e_i) + e_j \\ F_j\big(L_i(t^*), F_i(t^*, x^*)\big) = c_j(a_i t^* + e_i) + \mu_j(c_i t^* + \mu_i x^* + f_i) + f_j \end{cases} \tag{21}$$

When solving actual problems, the abscissa of point $\omega_j(\omega_i(P_0))$ is generally taken as an integer, denoting it as $P_0^{i,j}$, we get:

$$P_0^{i,j} = \big(\big[L_j\big(L_i(t^*)\big)\big], F_j\big(L_i(t^*), F_i(t^*, x^*)\big)\big) = (t_m, x_m^{i,j}) \tag{22}$$

where $[\cdot]$ is the rounding operation. For different i, the abscissa of $P_0^{i,j}$ may be the same. Thus, the value of the interpolation result x_m^j will be the average of the $P_0^{i,j}$ of those who have the same abscissa t_m:

$$x_m^j = \frac{1}{N}\sum_{i=1}^{N} F_j\big(L_i(t^*), F_i(t^*, x^*)\big) \tag{23}$$

This equation will be used in calculating $\Gamma(t, \Delta x') - \Gamma(t)$ and assessing the prediction error. Next, we are going to calculate the bias between $\Gamma(t, \Delta x')$ and $\Gamma(t)$.

Bias caused by endpoint disturbance

While forecasting the time offsets by fractal function extension, the initial point $P_0(t^*, x^*)$ is mapped into $\omega_{N+1}(P_0)$ in the interval $[t_N, t_{N+1}]$ by ω_{N+1} first. Then, it is mapped into $\omega_j(\omega_{N+1}(P_0))$ in the interval $[t_{j-1}, t_j]$ by ω_j. Like the calculating process above, the fractal interpolation value $P_0^{N+1,j}$ after a rounding operation is

$$P_0^{N+1,j} = \big(\big[L_j\big(L_{N+1}(t^*)\big)\big], F_j\big(L_{N+1}(t^*), F_{N+1}(t^*, x^*)\big)\big) = (t_m, x_m^{N+1,j}) \tag{24}$$

The value of the interpolation result $\tilde{x}_m^j$ in the prediction process is:

$$\tilde{x}_m^j = \frac{1}{N+1}\sum_{i=1}^{N+1} F_j\big(L_i(t^*), F_i(t^*, x^*)\big) \tag{25}$$

Thus, the interpolation bias between $\Gamma(t, \tilde{x}_{N+1})$ and $\Gamma(t)$, denote as $\Delta\Gamma$, is defined as:

$$\Delta\Gamma = \sqrt{\frac{1}{N}\sum_{j=1}^{N}\left(\tilde{x}_m^j - x_m^j\right)^2} \tag{26}$$

Next, we will prove the existence and uniqueness of the minimum value of the interpolation bias $\Delta\Gamma$ defined by (26) with respect to the estimated endpoint variable $\tilde{x}_{N+1}$.

Proof of existence and uniqueness

First, denote the interpolation result in the prediction process as:

$$\tilde{x}_m^j = \frac{1}{N+1}\left(\sum_{i=1}^{N} F_j\left(L_i(t^*), F_i(t^*, x^*)\right) + F_j\left(L_{N+1}(t^*), F_{N+1}(t^*, x^*)\right)\right) \tag{27}$$

Subtract (23) from (27) to obtain:

$$\begin{aligned}
&\tilde{x}_m^j - x_m^j \\
&= \left(\frac{1}{N+1} - \frac{1}{N}\right)\sum_{i=1}^{N} F_j\left(L_i(t^*), F_i(t^*, x^*)\right) + \frac{1}{N+1}F_j\left(L_{N+1}(t^*), F_{N+1}(t^*, x^*)\right) \\
&= \frac{1}{N+1}\left[F_j\left(L_{N+1}(t^*), F_{N+1}(t^*, x^*)\right) - \frac{1}{N}\sum_{i=1}^{N} F_j\left(L_i(t^*), F_i(t^*, x^*)\right)\right] \\
&= \frac{1}{N+1}\left[\mu_j F_{N+1}(t^*, x^*) + \phi_j\left(L_{N+1}(t^*)\right) - \frac{1}{N}\sum_{i=1}^{N} F_j\left(L_i(t^*), F_i(t^*, x^*)\right)\right]
\end{aligned} \tag{28}$$

Because the last two terms inside the square brackets of the above equation does not contain $\tilde{x}_{N+1}$, we will calculate the first term inside the square brackets that contains $\tilde{x}_{N+1}$ to obtain:

$$\begin{aligned}
&\mu_j F_{N+1}(t^*, x^*) = \mu_j\left(c_{N+1}t^* + \mu_{N+1}x^* + f_{N+1}\right) \\
&= \mu_j\left(\frac{\tilde{x}_{N+1} - x_N - \mu_{N+1}(\tilde{x}_{N+1} - x_0)}{t_{N+1} - t_0}t^* + \mu_{N+1}x^* + \frac{t_{N+1}x_N - t_0\tilde{x}_{N+1} - \mu_{N+1}(t_{N+1}x_0 - t_0\tilde{x}_{N+1})}{t_{N+1} - t_0}\right) \\
&= \mu_j\left(\frac{\tilde{x}_{N+1}t^* - x_N t^* - \mu_{N+1}t^*(\tilde{x}_{N+1} - x_0) + t_{N+1}x_N - t_0\tilde{x}_{N+1} - \mu_{N+1}(t_{N+1}x_0 - t_0\tilde{x}_{N+1})}{t_{N+1} - t_0} + \mu_{N+1}x^*\right) \\
&= \mu_j\left(\frac{\tilde{x}_{N+1}\left(t^* - \mu_{N+1}t^* - t_0 + \mu_{N+1}t_0\right) - x_N t^* + \mu_{N+1}t^*x_0 + t_{N+1}x_N - \mu_{N+1}t_{N+1}x_0}{t_{N+1} - t_0} + \mu_{N+1}x^*\right) \\
&= \mu_j\left(\frac{\tilde{x}_{N+1}(t^* - t_0)(1 - \mu_{N+1}) + (t_{N+1} - t^*)(x_N - \mu_{N+1}x_0)}{t_{N+1} - t_0} + \mu_{N+1}x^*\right) \\
&= \mu_j\lambda(1 - \mu_{N+1})\tilde{x}_{N+1} + \mu_j\left((1 - \lambda)(x_N - \mu_{N+1}x_0) + \mu_{N+1}x^*\right)
\end{aligned} \tag{29}$$

where $\lambda = \left(t^* - t_0\right)/\left(t_{N+1} - t_0\right)$. Denote α_j and β_j as:

$$\begin{cases}
\alpha_j = \mu_j\lambda(1 - \mu_{N+1}) \\
\beta_j = \mu_j\left((1 - \lambda)(x_N - \mu_{N+1}x_0) + \mu_{N+1}x^*\right) \\
\qquad + \phi_j\left(L_{N+1}(t^*)\right) - \dfrac{1}{N}\displaystyle\sum_{i=1}^{N} F_j\left(L_i(t^*), F_i(t^*, x^*)\right)
\end{cases} \tag{30}$$

we have:

$$\tilde{x}_m^j - x_m^j = \frac{\alpha_j\tilde{x}_{N+1} + \beta_j}{N+1} \tag{31}$$

Then, the square of the interpolation bias $\Delta\Gamma$ is:

$$(\Delta\Gamma)^2 = \frac{1}{N}\sum_{j=1}^{N}\left(\frac{\alpha_j\tilde{x}_{N+1}+\beta_j}{N+1}\right)^2 = \frac{1}{N(N+1)^2}\left(\tilde{x}_{N+1}^2\sum_{j=1}^{N}\alpha_j^2 + 2\tilde{x}_{N+1}\sum_{j=1}^{N}\alpha_j\beta_j + \sum_{j=1}^{N}\beta_j^2\right) \tag{32}$$

Thus, $(\Delta\Gamma)^2$ meets the minimum value when

$$\tilde{x}_{N+1} = -\frac{\sum_{j=1}^{N}\alpha_j\beta_j}{\sum_{j=1}^{N}\alpha_j^2} \tag{33}$$

and so does $\Delta\Gamma$. This completes the existence and uniqueness proof.

Endpoint based optimal fractal prediction algorithm

According to the previous discussion, the optimization model is given as:

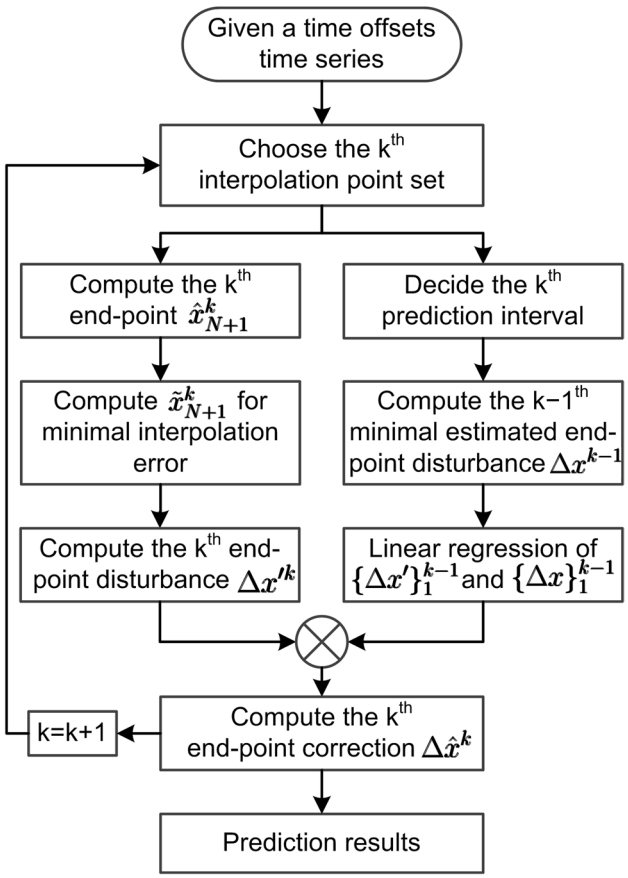

Fig. 11 Computing flow of the endpoint based optimal fractal prediction algorithm

$$\min\ \Delta\Gamma(\tilde{x}_{N+1}) = \frac{\sqrt{N}}{N(N+1)}\sqrt{\tilde{x}_{N+1}^2\sum_{j=1}^{N}\alpha_j^2 + 2\tilde{x}_{N+1}\sum_{j=1}^{N}\alpha_j\beta_j + \sum_{j=1}^{N}\beta_j^2} \tag{34}$$

where the parameters α_j and β_j are defined as in (30). Then, the algorithm for computing the estimated endpoint for BDS time offsets by fractal prediction is obtained and its computing flow is shown in Fig. 11.

Figure 11 illustrates the processing diagram of the BDS time offsets prediction algorithm using endpoint-based optimal fractal interpolation. Considering the current estimated endpoint for the minimal interpolation error and the endpoint estimation for the minimal prediction error, we divide this forecasting algorithm into two steps. The first step computes the estimated endpoint $\tilde{x}_{N+1}$ using (34) and obtains the disturbance $\Delta x'$ of $\hat{x}_{N+1}$ according to Han et al. (2018). The second step computes the current endpoint disturbance estimation Δx using the current estimated $\Delta x'$ and the linear relationship between the previous disturbance series $\{\Delta x'\}_1^{k-1}$ and $\{\Delta x\}_1^{k-1}$. Thus, the estimated endpoint-based optimization model to predict BDS time offsets has been built. The prediction accuracy of this model will be verified in the following section by comparing it with the prediction residuals using other models. A more detailed computing process can be found in the appendix.

Numerical tests and prediction accuracy discussion

The prediction effect of the proposed algorithm will be tested by comparing its prediction error with that of the linear/quadratic model with two periodic terms and the standard fractal interpolation forecasting model (shown in Fig. 7). The prediction lengths are 1 h, 3 h, 6 h, and 12 h. After that, the [UTC(NTSC)-BDT] series will be transformed into the [UTCr-BDT] to meet the requirement of GNSS interoperability; and the uncertainty of the corresponding prediction result is given.

Fitting length in the prediction process

When using the proposed algorithm or the standard fractal model, the fitting length, i.e. the interpolation interval, can be determined according to the memory span of a time series; and it is always taken as an integer multiple of the memory span. In this study, the fitting length of forecasting for [UTC(NTSC)-BDT] is 10 times its memory span.

When using the linear/quadratic prediction model, the fitting length of historical data affects the prediction accuracy directly (Vernotte et al. 2001). To verify the high precision of the proposed prediction model, we will choose the fitting length of the linear/quadratic model that achieves the

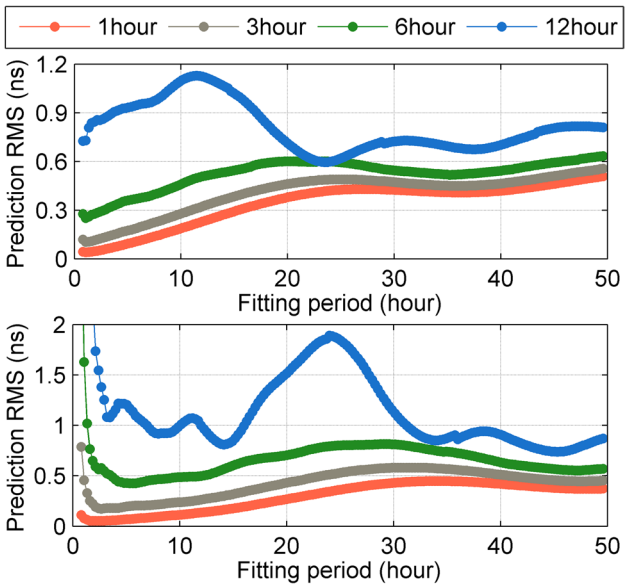

Fig. 12 Curves of prediction error of [UTC(NTSC)-BDT] quadratic model prediction with different fitting lengths. Top: Prediction error curves of linear model. Bottom: Prediction error curves of quadratic model

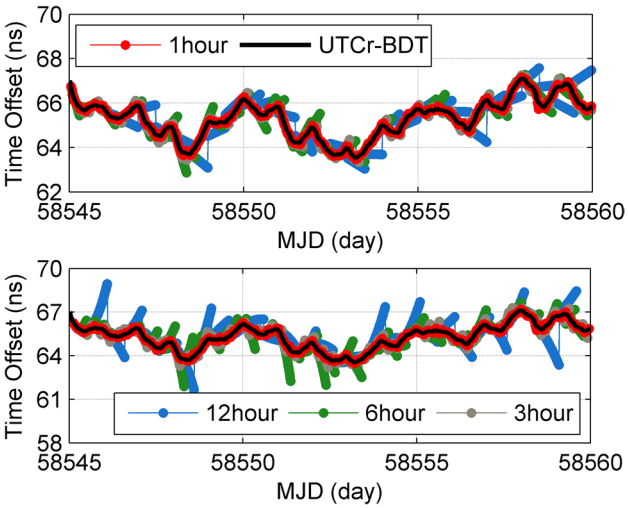

Fig. 13 Prediction results of [UTC(NTSC)-BDT] using the linear/quadratic model with two periodic terms added. Top: Prediction results of linear model. Bottom: Prediction results of quadratic model

minimal prediction error. Denote $\varepsilon(l)$ as the RMS of the prediction residual of fitting length l in the linear/quadratic model. The selected fitting length l_0 satisfies:

$$\varepsilon(l_0) = \min\{\varepsilon(l)\} \tag{35}$$

The curves of $\varepsilon(l)$ versus l in the [UTC(NTSC)-BDT] linear/quadratic prediction model over different prediction lengths are shown in Fig. 12. Using these fitting lengths to predict the [UTC(NTSC)-BDT] with a linear/quadratic model and adding two periodic terms, the prediction results are shown in Fig. 13. The divergence of prediction error is clearly seen in the figure, especially in long-term prediction situations.

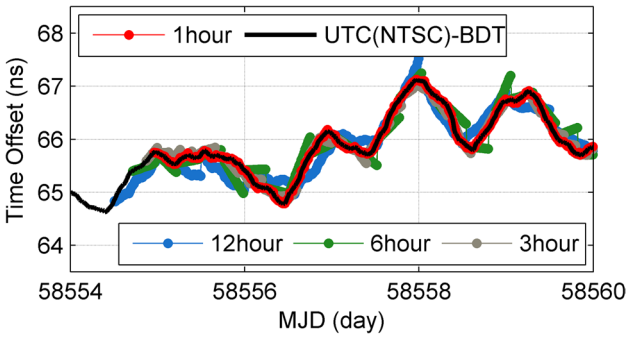

Fig. 14 Prediction results of [UTC(NTSC)-BDT] using the endpoint based optimal fractal interpolation prediction model; forecast spans are 1 h, 3 h, 6 h, and 12 h; fitting lengths of each forecast span are longer than 104 h, which is 10 times of the memory span calculated by (12)

Table 3 Selected fitting lengths and the corresponding prediction error of [UTC(NTSC)-BDT] forecasting using the different models with two periodic terms added

Model	Prediction lengths (h)	1	3	6	12
Linear	Selected fitting length (h)	1.067	1.067	1.067	23.467
	Prediction error (ns)	0.040	0.143	0.321	0.596
	Expected error (ns)	0.029	0.079	0.152	0.508
Quadratic	Selected fitting length (h)	2.933	2.933	5.867	45.600
	Prediction error (ns)	0.053	0.173	0.426	0.739
	Expected error (ns)	0.040	0.121	0.273	0.566
Standard FP	Prediction error (ns)	0.036	0.124	0.312	0.473
	Expected error (ns)	0.025	0.083	0.228	0.326
Optimal FP	Prediction error (ns)	0.020	0.082	0.191	0.284
	Expected error (ns)	0.014	0.060	0.124	0.194

The fitting length of both standard and optimal FP (fractal prediction model) is 10.4 h

Table 4 Relative accuracy improvements in percent of the endpoint based optimal fractal model compared with the quadratic model and standard fractal model

Model	1 h	3 h	6 h	12 h	Average
Linear	50.00	42.66	40.50	52.35	46.38
Quadratic	62.26	52.60	55.16	61.57	57.90
Standard FP	44.44	33.87	38.78	39.96	39.26

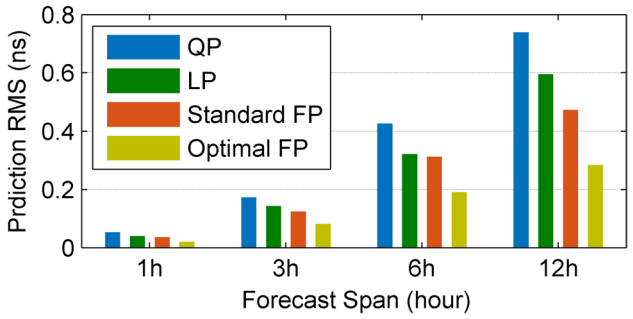

Fig. 15 Predicted RMS of [UTC(NTSC)-BDT] using different models with different forecast spans (QP = quadratic prediction model, LP = linear prediction model, FP = fractal prediction model)

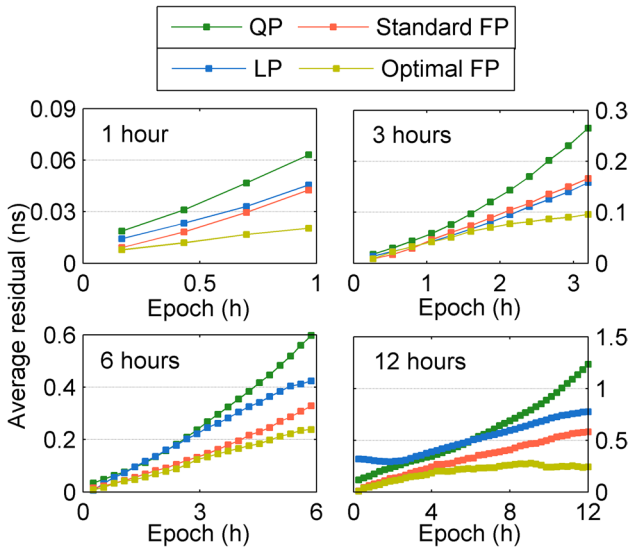

Fig. 16 Curves of average prediction RMS of each model in different forecast spans (QP = quadratic prediction model, LP = linear prediction model, FP = fractal prediction model)

The prediction results of [UTC(NTSC)-BDT] using the endpoint based optimal fractal interpolation prediction algorithm is shown in Fig. 14. Compared with the standard fractal interpolation prediction model and the quadratic models (shown in Table 3), the proposed model has more precise prediction results than the others (see Table 4 and Fig. 15). The fitting lengths of the two fractal models are both 10.4 h, the memory span of [UTC(NTSC)-BDT] obtained by equation (12). Notice that the expected error in Table 3 is the mean value of extrapolated the fit forward in each forecast period using the full parameter matrix.

It can be seen from Fig. 15 that the order of prediction error is Optimal FP < Standard FP < LP < QP. The prediction model proposed in this study has more precise prediction results than the quadratic model and the standard fractal model. From Table 4, it is found that the prediction accuracy improvement of the proposed model is almost 60% compared with the quadratic model and almost 40% compared with the standard fractal model. We have not explored the comparable prediction accuracy of a properly tuned Kalman filter involving linear, quadratic, 12 h, and 24 h terms in the presence of random walk noise; that will be the subject of a later work.

As we know, the prediction error increases as the forecast span increases. The proposed model not only improves the prediction accuracy but also restrains the increasing rate of prediction error with the increasing of the forecast span. To evaluate the inhibition of error divergence in each model, the average prediction RMS δ_i is considered; the specific formula is:

$$\delta_i = \sqrt{\frac{1}{m}\sum_{j=1}^{m} \delta x_{i,j}^2} \tag{36}$$

where $\delta x_{i,j}$ is the prediction residual at epoch i of the jth forecast span and m is the total number of the forecast span. Thus, the curve of δ_i will illustrate the average prediction error level with the increase in forecast epoch.

Figure 16 shows the δ_i curves of different models. It is clear that the proposed endpoint based optimal fractal prediction model does restrain the divergence of the prediction error as the forecast epoch incenses. The increase rate of prediction error in the proposed model is the lowest of the three.

BDT offsets prediction at GNSS interoperability level

However, the [UTC(NTSC)-BDT] time series does not meet the requirements for GNSS interoperability. The GNSS interoperability requires each system to transfer their timescales into a unique timescale, just like the UTC-GPS time offsets and UTC-GLONASS time offsets (denote as [UTC-GPST] and [UTC-GLOT] respectively) broadcasted by BIPM. To enhance the usability of BDT time offsets at interoperability level, the [UTC(NTSC)-BDT] should be transferred into UTC-BDT time offsets, denote as [UTC-BDT], using UTC-UTC(NTSC) time offsets:

$$[\text{UTC-BDT}] = [\text{UTC-UTC(NTSC)}] + [\text{UTC(NTSC)-BDT}] \tag{37}$$

However, equation (37) has only theoretical significance rather than practical application value. The [UTC-UTC(NTSC)] series is reported by the BIPM on a 5-day grid for MJD, which is quite different from the one-day data interval of the [UTC-GPST] and [UTC-GLOT]. The model error will transfer if we use the interpolation method to estimate the data from daily [UTC-UTC(NTSC)].

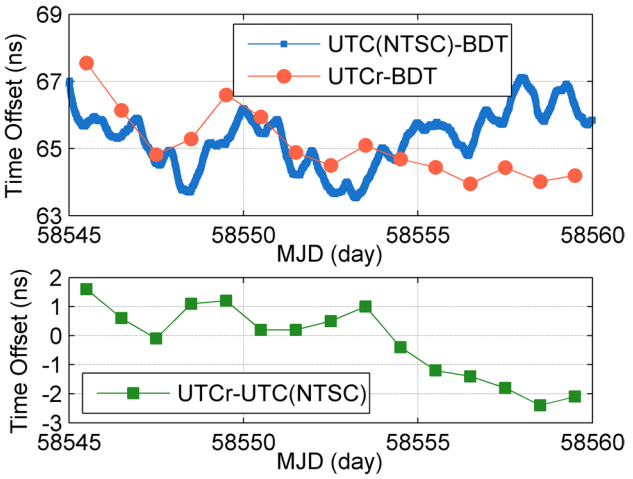

Fig. 17 [UTCr-BDT] series obtained by equation (38). Top: The [UTCr-BDT] series. Bottom: The [UTCr-UTC(NTSC)] series from MJD 58,545 to 58,559 is download from BIPM website

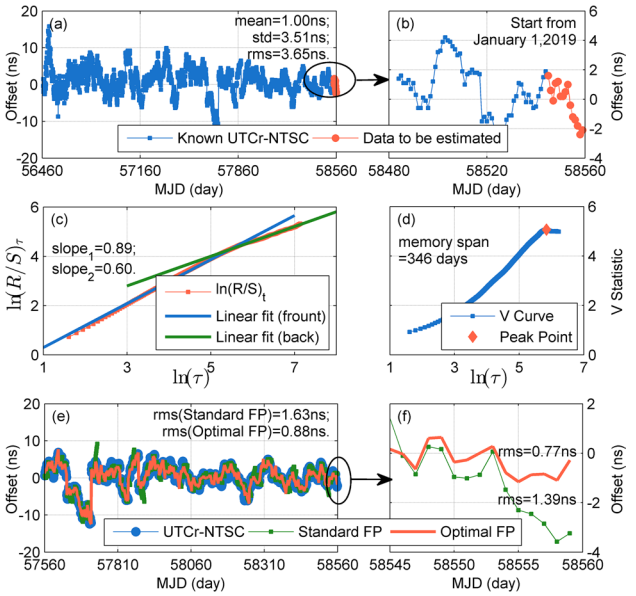

Fig. 18 Original series, fractal behavior detecting results, and prediction error series of [UTCr-UTC(NTSC)]. **a**: The [UTCr-UTC(NTSC)] series from MJD 56,467 to 58,559, the data to be forecasted is the last 14 days. **b**: The [UTCr-UTC(NTSC)] series start from January 1, 2019. **c**: The rescaled range analysis result of [UTCr-UTC(NTSC)], the regression line before and after the memory span show different slopes. **d**: The V statistic curve of [UTCr-UTC(NTSC)], the abscissa the peak point is 5.844 (≈ln345). **e**: The prediction result using standard and optimal fractal prediction model of the whole forecasting interval. **f**: The prediction error curve of both standard and optimal fractal prediction models during MJD 58,545–58,559

Therefore, the rapid realization of UTC (UTCr) is considered to replace UTC in this section, because the frequency of [UTCr-UTC(NTSC)] data, published by BIPM, is one day. The formula for [UTCr-BDT] is,

$$_i = [\text{UTCr-UTC(NTSC)}]_i + \text{mean}\left([\text{UTC(NTSC)-BDT}]_i\right) \quad (38)$$

The subscript i in equation (38) denotes the i th day of the given time offsets series; $\text{mean}\left([\text{UTC(NTSC)-BDT}]_i\right)$ is the mean value of [UTCr-UTC(NTSC)] in the ith day. The transformed [UTCr-BDT] series is shown in Fig. 17.

The simulated [UTCr-BDT] series shown in Fig. 17 is obtained from equation (38), the sum of the daily mean value of [UTC(NTSC)-BDT], and the [UTCr-UTC(NTSC)] value. The uncertainty of [UTCr-UTC(NTSC)] is not given by BIPM; and that of [UTC-UTC(NTSC)] during the same period reported in Circular T (T386) is about 2.6 ns. If we replace the uncertainty of [UTCr-UTC(NTSC)] with that of [UTC-UTC(NTSC)], the uncertainty of [UTCr-BDT] obtained from equation (38) during MJD 58,545–58,559 is estimated as $\sqrt{4.59^2 + 2.6^2} \approx 5.28$ ns. The actual uncertainty of [UTCr-BDT] is bigger than this value.

UTCr-NTCS offsets prediction

Forecasting the [UTCr-BDT] series in Fig. 17 is actually predicting both [UTCr-UTC(NTSC)] and [UTC(NTSC)-BDT] series. Since the BIPM reports UTCr once a week, the prediction length of [UTCr-UTC(NTSC)] here will be 7 days to meet the requirement of real-time application. Therefore, a longer [UTCr-UTC(NTSC)] series is required, which can be downloaded from the BIPM website; and we will use the fractal prediction method to predict this series. Before predicting, the fractal behavior of [UTCr-UTC(NTSC)] should be verified and its memory span should detected. After that, both standard and optimal fractal prediction model will be used to predict this series. The [UTCr-UTC(NTSC)] series, the fractal behavior detecting results, and the prediction error series are shown in Fig. 18.

As shown in Fig. 18a, the length of [UTCr-UTC(NTSC)] is 2093 days, started from July 2013 when BIPM began to report the UTCr offsets. The 77-days long [UTCr-UTC(NTSC)] series from January 1, 2019 is shown in Fig. 18b. Like all fractal series carrying long memory, the memory span of [UTCr-UTC(NTSC)] is about 345 days shown as the peak point in Fig. 18d; and the slopes of regression lines of $\ln \tau \sim \ln (R/S)_\tau$ curve before and after the memory span are 0.893 and 0.602, respectively, shown as Fig. 18c. Thus, the fractal behavior of [UTCr-UTC(NTSC)] series is verified according to Fig. 18c and d. The prediction results using both standard and optimal fractal prediction model are shown in Fig. 18e; the prediction accuracy of the optimal fractal prediction model has an improvement of more than 40% compared with the standard fractal prediction model. Moreover, the prediction residuals using the two

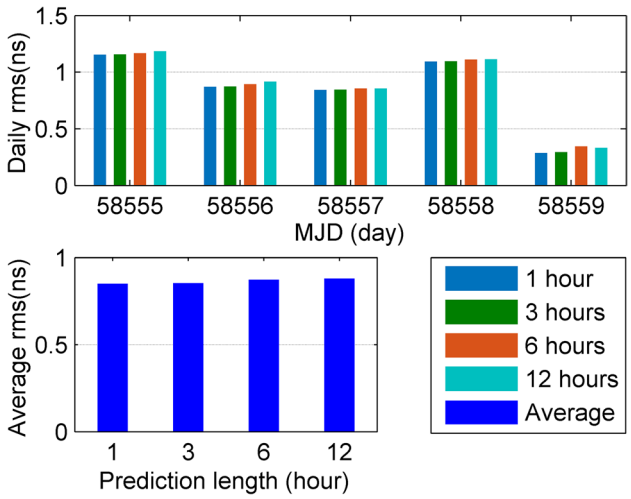

Fig. 19 Prediction results of [UTCr-BDT] using optimal fractal prediction method. Top: The RMS of the prediction residual in each day of different prediction length. Bottom: The average RMS of the prediction residual of different prediction length

models during MJD 58,545–58,559 are shown as Fig. 18f. Next, the prediction results of [UTC(NTSC)-BDT] and [UTCr-UTC(NTSC)] will be combined together to obtain the [UTCr-BDT] prediction value.

UTCr-BDT offsets prediction

The predicted [UTCr-BDT] offsets in a given day is composed of the predicted [UTCr-UTC(NTSC)] value of the day and the mean value of predicted [UTC(NTSC)-BDT] in this day. Therefore, the [UTCr-BDT] prediction results are obtained and are shown in Fig. 19. The RMS of prediction residual is computed as the following formula:

$$r = \sqrt{r_1^2 + r_2^2} \tag{39}$$

r_1 and r_2 refers to the prediction residual RMS of [UTCr-UTC(NTSC)] and [UTC(NTSC)-BDT] respectively; and r denotes the RMS of [UTCr-BDT] prediction residual.

As shown in Fig. 19, the prediction accuracies of [UTCr-BDT] are no more than 1 ns, and their differences are small when the prediction length changes. The variance of [UTC(NTSC)-BDT] is about 0.86 ns and the prediction accuracies are no more than 0.3 ns; the variance of [UTCr-UTC(NTSC)] series is almost 4 ns; and the 7-days long prediction accuracy is about 0.77 ns. Therefore, the prediction error of [UTCr-BDT] series contributed by [UTCr-UTC(NTSC)] is bigger than that by [UTC(NTSC)-BDT]. The main reason is that the variance of the original [UTCr-UTC(NTSC)] series is bigger than [UTC(NTSC)-BDT] series.

Discussion and conclusion

A system time offsets prediction model is necessary according to the requirements of GNSS interoperability. Since the system time offsets is different from clock offsets, the prediction modeling should be processed according to its statistical characteristics. Thus, the fractal prediction model is proposed based on the fractal behavior of system time offsets. Some methods and conclusions can be summarized as follows:

(1) It is mathematically proven that the [UTC(NTSC)-BDT] is a fractal time series with a memory span of 10.4 h. In system offsets prediction, the fitting length should be an integer multiple of the memory span.
(2) The fractal interpolation prediction error is related to the value of the estimated endpoint. One of the most important conclusions of this research is that there is a correlation between the estimated endpoints with minimal interpolation error and minimal prediction error. The other one is that the estimated endpoint with minimal interpolation error exists and is unique.
(3) Based on the results above, we proposed the endpoint based optimal fractal prediction model of BDS-3 time offsets forecasting. Using the 15-day BDS-3 time offsets observation provided by the NTCS, the average prediction accuracy of the proposed prediction improves by 57.90% and 39.26% compared to that of a quadratic model and standard fractal prediction model, respectively.
(4) The proposed prediction model not only has high prediction accuracy, but also has the ability to restrain the divergence of the prediction error as the forecast epoch increases. This shows that the proposed prediction model will improve the stability of long-term prediction.

Appendix: Specific calculation process of fractal interpolation bias

The main purpose of this appendix is to provide the specific computing process of parameter β_j. This will help us ensure the existence and uniqueness of the estimated endpoint disturbance for minimal interpolation error.

First, we will simplify the parameters defined by equation (16). Since the interpolation series $\{t_i\}$ $(i = 0, 1, \cdots, N)$ is always an arithmetic progression, we have:

$$\begin{cases} a_i = \dfrac{t_i - t_{i-1}}{t_N - t_0} = \dfrac{1}{N} \\ a_{N+1} = \dfrac{t_{N+1} - t_N}{t_{N+1} - t_0} = \dfrac{1}{N+1} \end{cases} \tag{40}$$

Then, the sums of e_i, c_i and f_i are calculated as follows:

$$\begin{aligned} \sum_{i=1}^{N} e_i &= \sum_{i=1}^{N} \frac{t_N t_{i-1} - t_0 t_i}{t_N - t_0} = \frac{1}{t_N - t_0} \sum_{i=1}^{N} \left(t_N t_{i-1} - t_0 t_i\right) \\ &= \frac{1}{t_N - t_0}\left(\sum_{i=1}^{N} t_N t_{i-1} - \sum_{i=1}^{N} t_0 t_i\right) = \frac{1}{t_N - t_0}\left(t_N \sum_{i=1}^{N} t_{i-1} - t_0 \sum_{i=1}^{N} t_i\right) \\ &= \frac{1}{t_N - t_0}\left[t_N\left(\sum_{i=0}^{N} t_i - t_N\right) - t_0\left(\sum_{i=0}^{N} t_i - t_0\right)\right] \\ &= \frac{1}{t_N - t_0}\left[\left(t_N - t_0\right)\sum_{i=0}^{N} t_i + t_0^2 - t_N^2\right] = \sum_{i=0}^{N} t_i - \left(t_N + t_0\right) \\ &= \left(t_N + t_0\right)\frac{N+1}{2} - \left(t_N + t_0\right) = \left(t_N + t_0\right)\frac{N-1}{2} \end{aligned} \tag{41}$$

$$\begin{aligned} \sum_{i=1}^{N} c_i &= \sum_{i=1}^{N} \frac{x_i - x_{i-1} - \mu_i(x_N - x_0)}{t_N - t_0} = \sum_{i=1}^{N} \frac{x_i - x_{i-1}}{t_N - t_0} - \frac{(x_N - x_0)}{t_N - t_0} \sum_{i=1}^{N} \mu_i \\ &= \frac{x_N - x_0}{t_N - t_0} - \frac{x_N - x_0}{t_N - t_0} \sum_{i=1}^{N} \mu_i = \frac{x_N - x_0}{t_N - t_0}\left(1 - \sum_{i=1}^{N} \mu_i\right) \end{aligned} \tag{42}$$

$$\begin{aligned} \sum_{i=1}^{N} f_i &= \sum_{i=1}^{N} \frac{t_N x_{i-1} - t_0 x_i - \mu_i(t_N x_0 - t_0 x_N)}{t_N - t_0} \\ &= \frac{1}{t_N - t_0}\left(t_N \sum_{i=1}^{N} x_{i-1} - t_0 \sum_{i=1}^{N} x_i - (t_N x_0 - t_0 x_N) \sum_{i=1}^{N} \mu_i\right) \\ &= \frac{1}{t_N - t_0}\left(t_N \sum_{i=0}^{N} x_i - t_N x_N - t_0 \sum_{i=0}^{N} x_i + t_0 x_0 - (t_N x_0 - t_0 x_N) \sum_{i=1}^{N} \mu_i\right) \\ &= \sum_{i=0}^{N} x_i + \frac{1}{t_N - t_0}\left(t_0 x_0 - t_N x_N - (t_N x_0 - t_0 x_N) \sum_{i=1}^{N} \mu_i\right) \\ &= \sum_{i=0}^{N} x_i - \left(\frac{x_N\left(t_N - t_0\right) + t_0\left(x_N - x_0\right)}{t_N - t_0} + \frac{x_0\left(t_N - t_0\right) - t_0\left(x_N - x_0\right)}{t_N - t_0} \sum_{i=1}^{N} \mu_i\right) \\ &= \sum_{i=0}^{N} x_i - x_N - t_0 \frac{x_N - x_0}{t_N - t_0} - \left(x_0 - t_0 \frac{x_N - x_0}{t_N - t_0}\right) \sum_{i=1}^{N} \mu_i \\ &= \sum_{i=0}^{N} x_i - x_N + x_0 - x_0 - t_0 \frac{x_N - x_0}{t_N - t_0} - \left(x_0 - t_0 \frac{x_N - x_0}{t_N - t_0}\right) \sum_{i=1}^{N} \mu_i \\ &= \sum_{i=0}^{N} x_i + \left(x_0 - t_0 \frac{x_N - x_0}{t_N - t_0}\right)\left(1 - \sum_{i=1}^{N} \mu_i\right) - x_N - x_0 \\ &= \sum_{i=1}^{N-1} x_i + \left(\frac{t_N x_0 - t_0 x_N}{t_N - t_0}\right)\left(1 - \sum_{i=1}^{N} \mu_i\right) \end{aligned} \tag{43}$$

For the parameter e_{N+1}, we have:

$$\begin{aligned} e_{N+1} &= \frac{t_{N+1}t_N - t_0 t_{N+1}}{t_{N+1} - t_0} = \frac{t_{N+1}t_N - t_N t_0 + t_N t_0 - t_0 t_{N+1}}{t_{N+1} - t_0} \\ &= \frac{t_N\left(t_{N+1} - t_0\right) + t_0\left(t_N - t_{N+1}\right)}{t_{N+1} - t_0} = t_N - \frac{t_0}{N+1} \end{aligned} \tag{44}$$

According to equation (31), the expression of β_j contains two parts:

$$\begin{aligned} \beta_j = & \underbrace{\mu_j\left((1-\lambda)(x_N - \mu_{N+1}x_0) + \mu_{N+1}x^*\right)}_{\text{Part I}} \\ & \underbrace{+\phi_j\left(L_{N+1}(t^*)\right) - \frac{1}{N}\sum_{i=1}^{N} F_j\left(L_i(t^*), F_i(t^*, x^*)\right)}_{\text{Part II}} \end{aligned} \tag{45}$$

Since Part I of β_j is already simplified, we will focus on the last part. According to (15):

$$\begin{aligned} & \phi_j\left(L_{N+1}(t^*)\right) - \frac{1}{N}\sum_{i=1}^{N} F_j\left(L_i(t^*), F_i(t^*, x^*)\right) \\ &= \phi_j\left(L_{N+1}(t^*)\right) - \frac{1}{N}\sum_{i=1}^{N}\left(\phi_j\left(L_i(t^*)\right) + \mu_j F_i(t^*, x^*)\right) \\ &= \frac{1}{N}\sum_{i=1}^{N}\phi_j\left(L_{N+1}(t^*)\right) - \frac{1}{N}\sum_{i=1}^{N}\phi_j\left(L_i(t^*)\right) - \frac{1}{N}\sum_{i=1}^{N}\mu_j F_i(t^*, x^*) \\ &= \frac{1}{N}\sum_{i=1}^{N}\left[\phi_j\left(L_{N+1}(t^*)\right) - \phi_j\left(L_i(t^*)\right)\right] - \frac{\mu_j}{N}\sum_{i=1}^{N} F_i(t^*, x^*) \end{aligned} \tag{46}$$

For the first segment of (46), using (40), (41) and (44), we obtain:

$$\begin{aligned} & \frac{1}{N}\sum_{i=1}^{N}\left[\phi_j\left(L_{N+1}(t^*)\right) - \phi_j\left(L_i(t^*)\right)\right] \\ &= \frac{1}{N}\sum_{i=1}^{N}\left(c_j L_{N+1}(t^*) + f_j - c_j L_i(t^*) - f_j\right) = \frac{c_j}{N}\sum_{i=1}^{N}\left(L_{N+1}(t^*) - L_i(t^*)\right) \\ &= \frac{c_j}{N}\sum_{i=1}^{N}\left(a_{N+1}t^* + e_{N+1} - a_i t^* - e_i\right) \\ &= \frac{c_j}{N}\left[t^*\left(\sum_{i=1}^{N} a_{N+1} - \sum_{i=1}^{N} a_i\right) + \sum_{i=1}^{N} e_{N+1} - \sum_{i=1}^{N} e_i\right] \\ &= \frac{c_j}{N}\left[t^*\left(\frac{N}{N+1} - 1\right) + N\left(t_N - \frac{t_0}{N+1}\right) - \left(t_N + t_0\right)\frac{(N-1)}{2}\right] \\ &= \frac{c_j}{N}\left(-\frac{t^*}{N+1} + N t_N - \frac{N t_0}{N+1} - \frac{(N-1)t_N}{2} - \frac{(N-1)t_0}{2}\right) \\ &= \frac{c_j}{N}\left(-\frac{t^*}{N+1} + \frac{N+1}{2}t_N - \frac{N t_0}{N+1} - \frac{(N+1)t_0}{2} + t_0\right) \\ &= \frac{c_j}{N}\left(\frac{t_0 - t^*}{N+1} + \frac{N+1}{2}\left(t_N - t_0\right)\right) \end{aligned} \tag{47}$$

For the second segment of (46), using (42) and (43), we obtain:

$$\begin{aligned}
\sum_{i=1}^{N} F_i(t^*,x^*) &= \sum_{i=1}^{N} c_i t^* + \sum_{i=1}^{N} \mu_i x^* + \sum_{i=1}^{N} f_i \\
&= t^* \sum_{i=1}^{N} c_i + x^* \sum_{i=1}^{N} \mu_i + \sum_{i=1}^{N} f_i \\
&= t^* \frac{x_N - x_0}{t_N - t_0}\left(1 - \sum_{i=1}^{N} \mu_i\right) + x^* \sum_{i=1}^{N} \mu_i + \sum_{i=1}^{N-1} x_i + \left(\frac{t_N x_0 - t_0 x_N}{t_N - t_0}\right)\left(1 - \sum_{i=1}^{N} \mu_i\right) \\
&= \left(\frac{t^*(x_N - x_0) + t_N x_0 - t_0 x_N}{t_N - t_0} - x^*\right)\left(1 - \sum_{i=1}^{N} \mu_i\right) + x^* + \sum_{i=1}^{N-1} x_i \\
&= \left(\frac{x_N(t^* - t_0) + x_0(t_N - t^*)}{t_N - t_0} - x^*\right)\left(1 - \sum_{i=1}^{N} \mu_i\right) + x^* + \sum_{i=1}^{N-1} x_i \\
&= \left(\eta x_N + (1-\eta)x_0 - x^*\right)\left(1 - \sum_{i=1}^{N} \mu_i\right) + x^* + \sum_{i=1}^{N-1} x_i
\end{aligned} \tag{48}$$

where $\eta = (t^* - t_0)/(t_N - t_0)$. Substituting results (46), (47) and (48) into (45), the specific expression of β_j is given as:

$$\begin{aligned}
\beta_j &= \mu_j\left((1-\lambda)(x_N - \mu_{N+1}x_0) + \mu_{N+1}x^*\right) \\
&\quad + \phi_j\left(L_{N+1}(t^*)\right) - \frac{1}{N}\sum_{i=1}^{N} F_j\left(L_i(t^*), F_i(t^*,x^*)\right) \\
&= \mu_j\left((1-\lambda)(x_N - \mu_{N+1}x_0) + \mu_{N+1}x^*\right) \\
&\quad + \frac{c_j}{N}\left(\frac{t_0 - t^*}{N+1} + \frac{N+1}{2}(t_N - t_0)\right) \\
&\quad - \frac{\mu_j}{N}\left[\left(\eta x_N + (1-\eta)x_0 - x^*\right)\left(1 - \sum_{i=1}^{N} \mu_i\right) + x^* + \sum_{i=1}^{N-1} x_i\right]
\end{aligned} \tag{49}$$

It is obvious that parameter β_j does not contain $\tilde{x}_{N+1}$. This completes the calculation of the fractal interpolation bias $\Delta\Gamma$.

Acknowledgements This study is supported by Shaanxi Postdoctoral research fund (No. 2017BSHEDZZ22), National Natural Science Fund of China (No. 41774025, 61976176).

Data Availability The datasets of [UTCr-UTC(NTSC)] analyzed during the current study are available in the BIPM repository, ftp://ftp2.bipm.org/pub/tai/Rapid-UTC/utcrlab/utcr-ntsc. The [UTC(NTSC)-BDT] data that support the findings of this study are available from NTSC CAS, but restrictions apply to the availability of these data, which were used under license for the current study, and so are not publicly available. Data are, however, available from the authors upon reasonable request and with permission of NTCS CAS.

References

Fu WJ, Zhang Q, Huang GW (2015) Analysis of combined real-time predicting model of BDS/GPS system time offset. J Geod Geodyn 35(4):653–657. https://doi.org/10.14075/j.jgg.2015.04.024

Gao WG, Jiao WH, Xiao Y, Wang ML, Yuan HB (2011) An evaluation of the Beidou time system (BDT). J Navig 64(S1):31–39. https://doi.org/10.1017/S0373463311000452

Guang W, Dong S, Wu WJ, Zhang JH, Yuan HB, Zhang SG (2018) Progress of BeiDou time transfer at NTSC. Metrologia 55(2):175–187. https://doi.org/10.1088/1681-7575/aaa673

Han T, Wu HT, Lu XC, Wang X, Bai Y, Hao WN, Yang G (2013) Research on GNSS Interoperable Parameters. In: Proceedings of ION Pacific PNT 2013, Institute of Navigation, Honolulu, Hawaii, USA, April 22–25, 115–122

Han T, Lu XC, Du J, Zhang XZ, Ji YQ (2017) Analysis of GNSS user/industry interoperability viewpoint survey results. Lect Notes Electr Eng 439:605–619. https://doi.org/10.1007/978-981-10-4594-3_51

Han T, Yang YX, Huang GW, Wu J (2018) Fractal behavior of GNSS time offsets and fractal interpolation forecasting method for multi-GNSS time synchronization. GPS Solut 22(4):97. https://doi.org/10.1007/s10291-018-0762-6

Huang GW, Zhang Q, Xu GC (2014) Real-time clock offset prediction with an improved model. GPS Solut 18(1):95–104. https://doi.org/10.1007/s10291-013-0313-0

Hurst HE (1951) Long term storage capacities of reservoirs. Trans Am Soc Civ Eng 116(12):776–808. https://doi.org/10.1234/12345678

ICG Secretariat (2019) Joint statement. In: 14th meeting of the International Committee on Global Navigation Satellite Systems, Bangalore, India, December 9–13. http://www.unoosa.org/documents/pdf/icg/2019/icg14/Joint_statement_ICG-14.pdf

Mazel DS, Hayes MH (1992) Using iterated function systems to model discrete sequences. IEEE Trans Signal Process 40(7):1724–1734. https://doi.org/10.1109/78.143444

Vernotte F, Delporte J, Brunet M, Tournier T (2001) Uncertainties of drift coefficients and extrapolation errors: application to

clock error prediction. Metrologia 38(4):325–342. https://doi.org/10.1088/0026-1394/38/4/6

Wu HT (2011) Time foundation in satellite navigation system. Science press, Beijing

Yang YX, Li JL, Xu JY et al (2011) Contribution of the Compass satellite navigation system to global PNT users. Chin Sci Bull 56(26):2813–2819. https://doi.org/10.1007/s11434-011-4627-4

Yang YX, Lu MQ, Han CH (2016) Some notes on interoperability of GNSS. Acta Geod Cartogr Sin 45(3):253–259. https://doi.org/10.11947/j.AGCS.2016.20150653

Yang YX, Gao WG, Guo SR, Mao Y, Yang YF (2019) Introduction to BeiDou-3 navigation satellite system. Navigation 66(1):1–12. https://doi.org/10.1002/navi.291

Zhang HJ, Li XH, Zhu L, Zhang X (2014a) Research on GNSS system time offset monitoring and prediction. Lect Notes Electr Eng 303(1):427–438. https://doi.org/10.1007/978-3-642-54737-9_37

Zhang JH, Yuan HB, Dong SW, Yin LL (2014b) Prediction of GNSS time difference based on combination of Grey model and quadratic polynomial model. J Time Freq 37(4):199–205. https://doi.org/10.13875/j.issn.1674-0637.2014-04-0199-07

Zhu L, Zhang HJ, Li XH, Ren Y, Xu LX (2016) Analyzing prediction methods and precision of GNSS system time offset using endpoint and Kalman filter. Lect Notes Electr Eng 390(3):661–671. https://doi.org/10.1007/978-981-10-0940-2_58

Tao Han is a researcher of Xi'an University of Technology, Xi'an, People's Republic of China. He worked as a postdoctoral researcher at the Chang'an University with cooperative tutor professor Yuanxi Yang during 2017–2019. Tao Han received his Bachelor and M.Sc. degrees in Applied Mathematics from Northwest University (China), in 2006 and 2009, and his Ph. D. degree in Instrument Science and Technology from National Time Service Center, Chinese Academy of Sciences, in 2016. His research activities include GNSS interoperability, multi-GNSS, and mathematical modeling in GNSS applications.

Decai Zou is a researcher of the National Time Service Center, Chinese Academy of Sciences (NTSC, CAS), Xi'an, People's Republic of China. He received M. Sc. and Ph. D. degrees in Telecommunication Technology from National Time Service Center, Chinese Academy of Sciences, in 2006 and 2009. His research activities include satellite navigation technology, theory and method.